Cell Reports, Volume *22*

Supplemental Information

Hidden Structural Modules in a Cooperative RNA Folding Transition

Brant Gracia, Hashim M. Al-Hashimi, Namita Bisaria, Rhiju Das, Daniel Herschlag, and Rick Russell

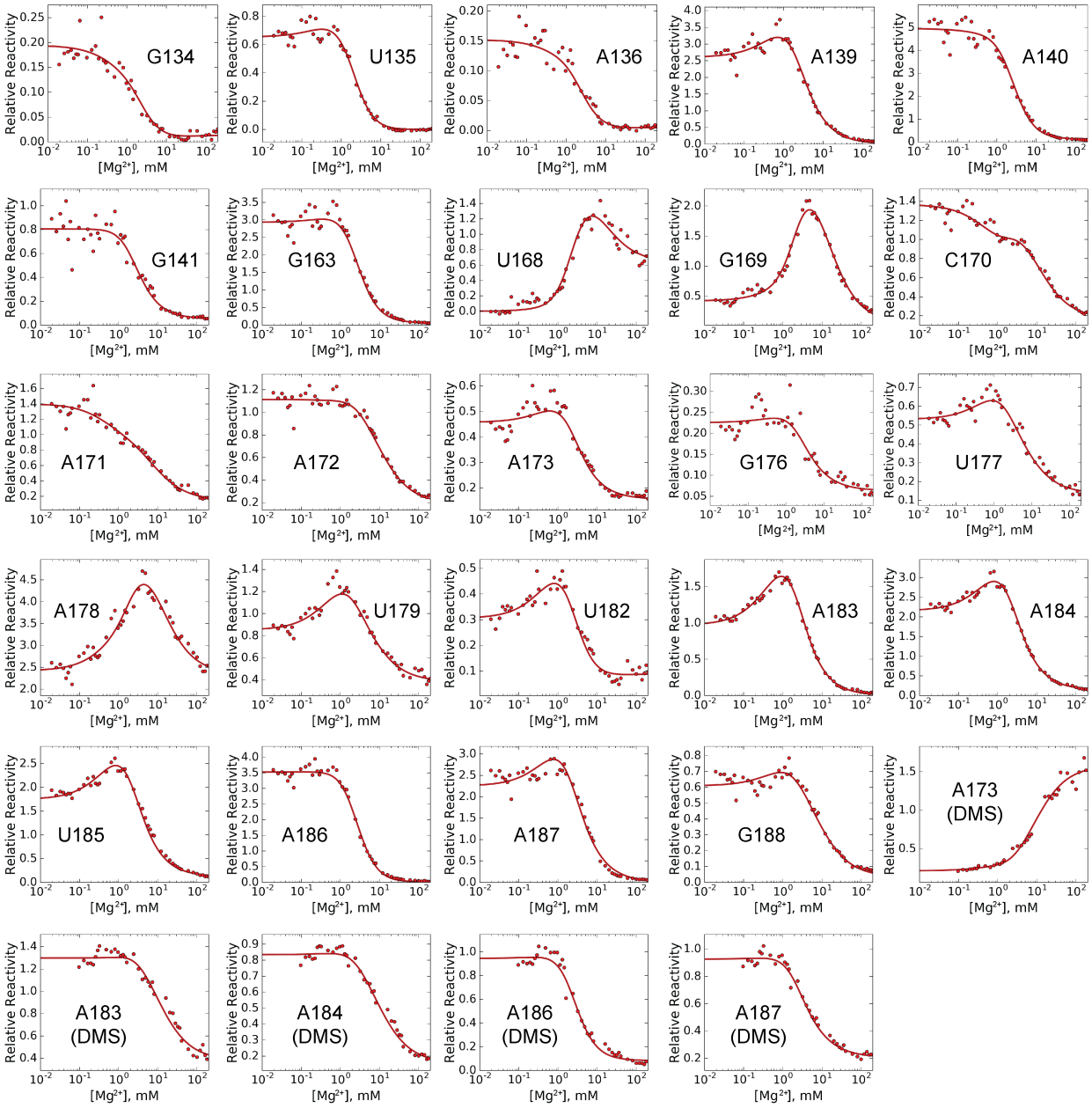

Figure S1. Global fitting of footprinting data in Kintek Global Kinetic Explorer. Related to Figure 3

Red dots indicate the footprinting data and the curve shows the best fit by a global model, which included four states and three transitions. See *Supplemental Experimental Procedures* for further details.

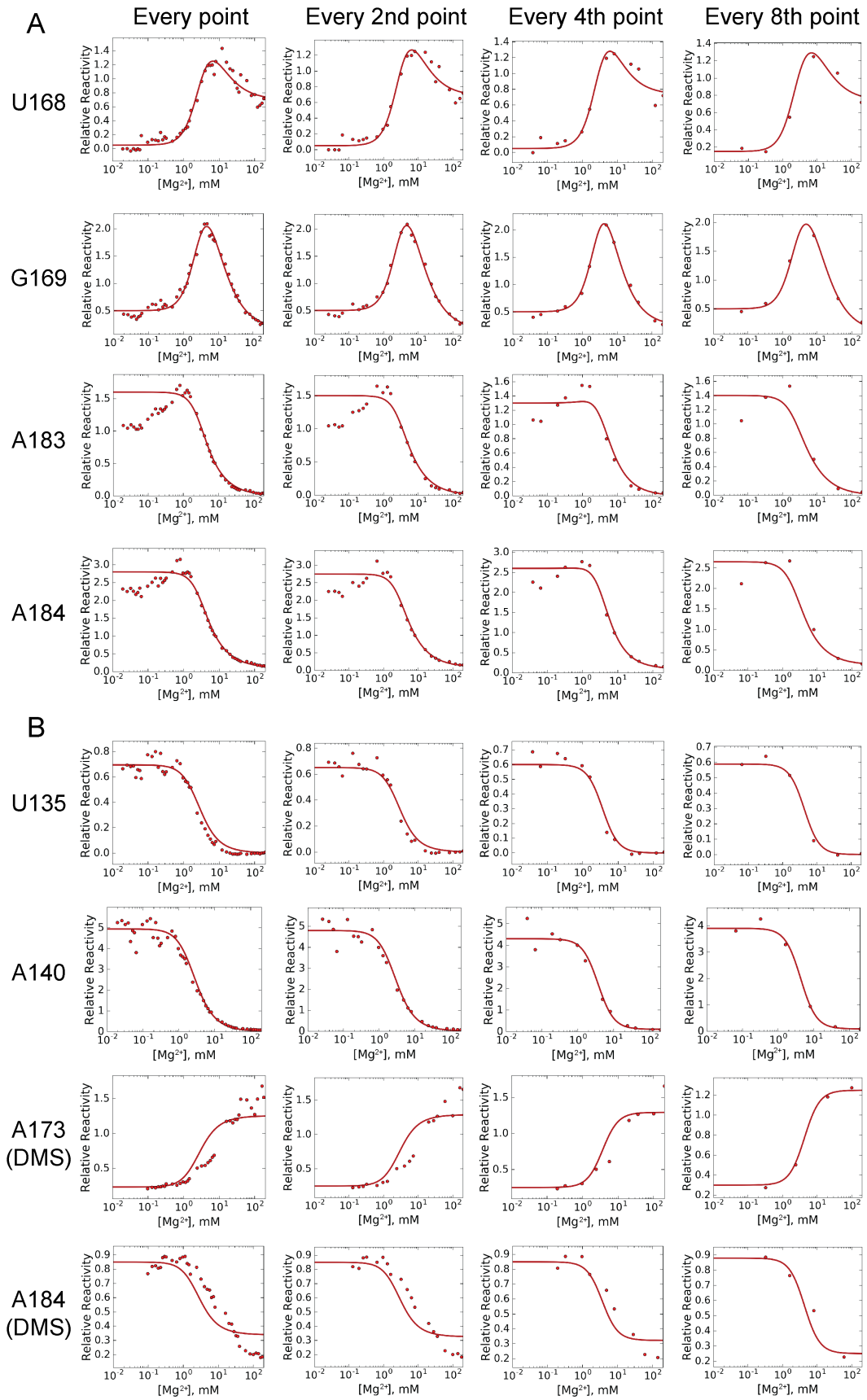
A
Every point
Every 2nd point
Every 4th point
Every 8th point
U168
G169
A183
A184
B
U135
A140
A173 (DMS)
A184 (DMS)
Relative Reactivity
[Mg2+], mM

Figure S2. Tests of global fitting using mock data sets with fewer points. Related to Figure 3

We performed a series of tests with subsets of the experimental data to determine whether the same global model would have been reached with data sets consisting of fewer points.

(A) Global fitting was performed using nucleotides with the largest and most descriptive signals for each of the three transitions. This test was performed using SHAPE data from U168, G169, A183, A184, and A186. (Results from A186 are not shown due to space constraints.) When the density of data is reduced by a factor of eight (right panels), the data can be adequately described with a model that includes the two Mg^{2+} dependent transitions that are the focus of this work, but the transition at low Mg^{2+} concentrations is omitted from the model.

(B) Global fitting was performed using nucleotides that give large signals for the two Mg^{2+}-dependent folding transitions, but with both transitions giving a change in the same direction rather than an increase followed by a decrease in signal at higher Mg^{2+} concentrations. This test was performed using SHAPE data from U135 and A140, as well as DMS data from A173, A184, and A186. (Results from A186 are not shown due to space constraints.) When these data are reduced in density, they can be adequately described by a model that includes only a single Mg^{2+}-dependent transition.

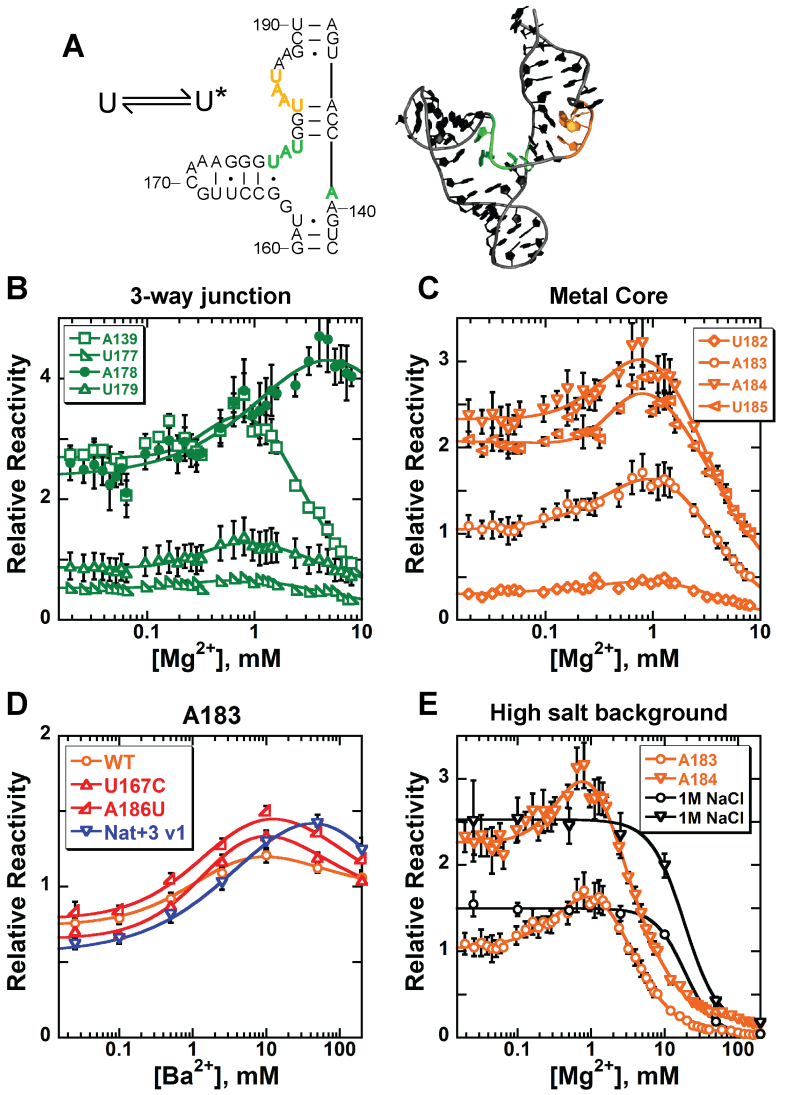

Figure S3. Reactivity enhancements at sub-millimolar Mg^{2+} concentrations depend on electrostatic environment and do not reflect formation of specific secondary or tertiary structures. Related to Figure 3
(A) 2D and 3D models indicating nucleotides that undergo SHAPE reactivity enhancements at low Mg^{2+} concentrations (U to U*). MC nucleotides are orange and 3WJ nucleotides are green.

(B–C) SHAPE reactivity profiles for nucleotides within the 3WJ (panel B) and the MC (panel C) that display enhancements in the Mg^{2+}-dependent transition from U to U*.

(D) Dependence of SHAPE reactivity of the MC nucleotide A183 in the presence of various concentrations of Ba^{2+}, which does not support MC formation (Travers et al., 2007). The enhancement at low Mg^{2+} remains present despite the lack of MC formation in Ba^{2+} for the wild type P5abc (orange circles). In addition, the reactivity profile of A183 is essentially unaffected by a mutation that blocks MC formation (A186U, red triangles), a mutation that stabilizes alternative structure in P5c and thereby weakens MC formation (U167C, red angled triangles), and a mutation that stabilizes the native secondary structure of P5c (Nat+3 v1, blue).

(E) SHAPE footprinting of the MC in the presence of 1 M NaCl (black). This high Na^{+} concentration results in electrostatic relaxation of the P5abc domain (Das et al., 2005), and we find that it eliminates the observed enhancements at sub-millimolar Mg^{2+} concentrations for A183 (black circles) and A184 (black triangles). Corresponding data under standard conditions are shown in orange for comparison.

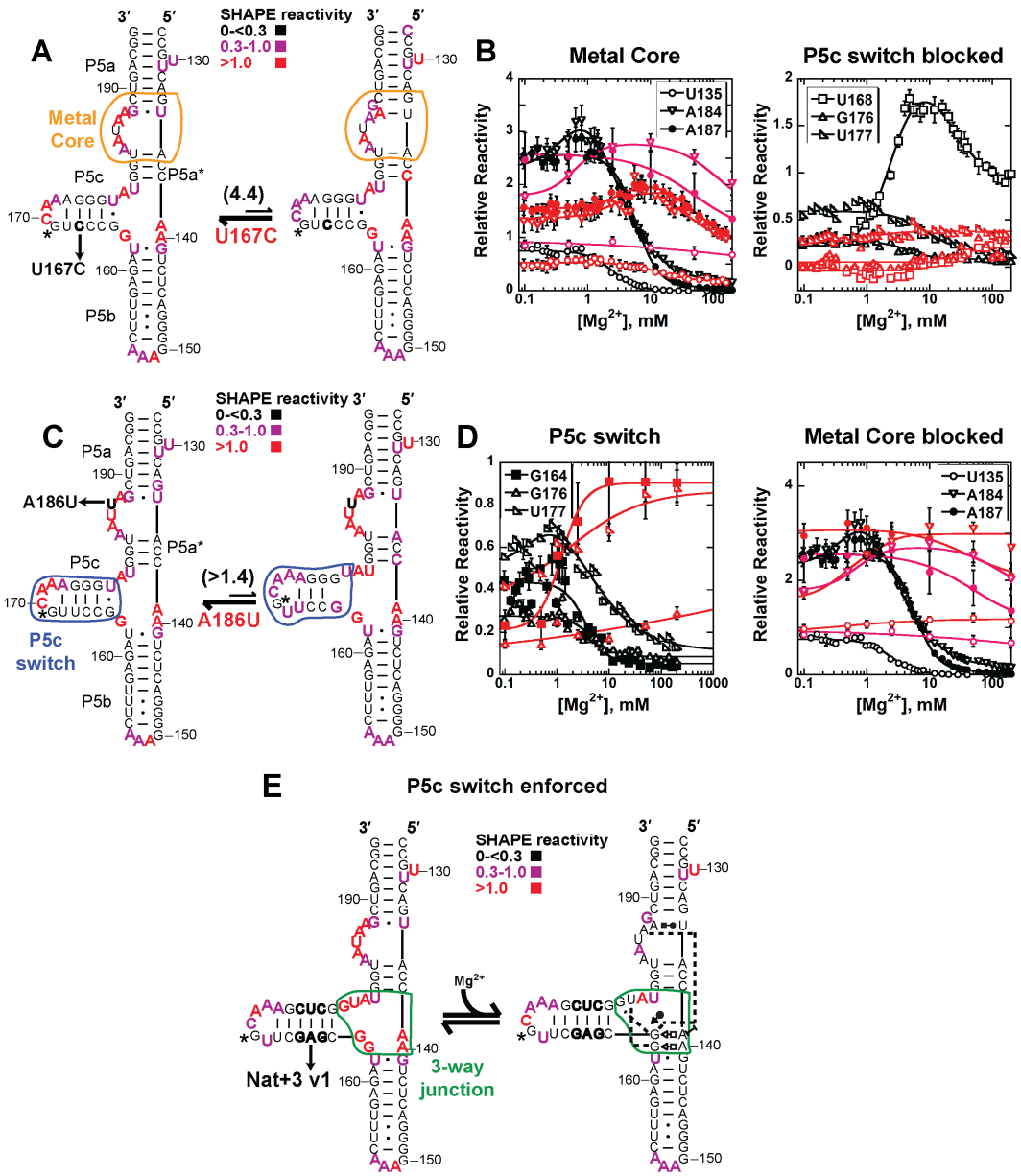

Figure S4. Cooperativity between the secondary structure switch in P5c and tertiary structure formation of the MC. Related to Figure 4

(A) SHAPE reactivity heat map of a mutant in which the alternative secondary structure of P5c is stabilized (U167C). Heat maps show reactivity of each nucleotide to SHAPE reagent in the absence and presence of saturating Mg^{2+} (50–200 mM Mg^{2+}). Nucleotides that have values between 0.3-1.0 are purple and those with values greater than 1.0 are red. The asterisk at position G169 indicates that this position displayed a substantial signal in the absence of the footprinting reagent, preventing analysis of this position.

(B) Mg^{2+}-concentration dependence of SHAPE reactivity for nucleotides in the 3WJ and MC (left) and in P5c (right) for the mutant U167C P5abc (red). Reactivity of the same nucleotides is shown also for the double mutant U167C/A186U (magenta) and the wild-type P5abc for reference (black).

(C–D) SHAPE reactivity heat maps and Mg^{2+}-concentration dependence for a mutant that blocks MC formation (A186U, red). Data are also shown for wild-type P5abc for comparison (black).

(E) SHAPE reactivity heat maps of a mutant that enforces the native P5c (Nat+3 v1).

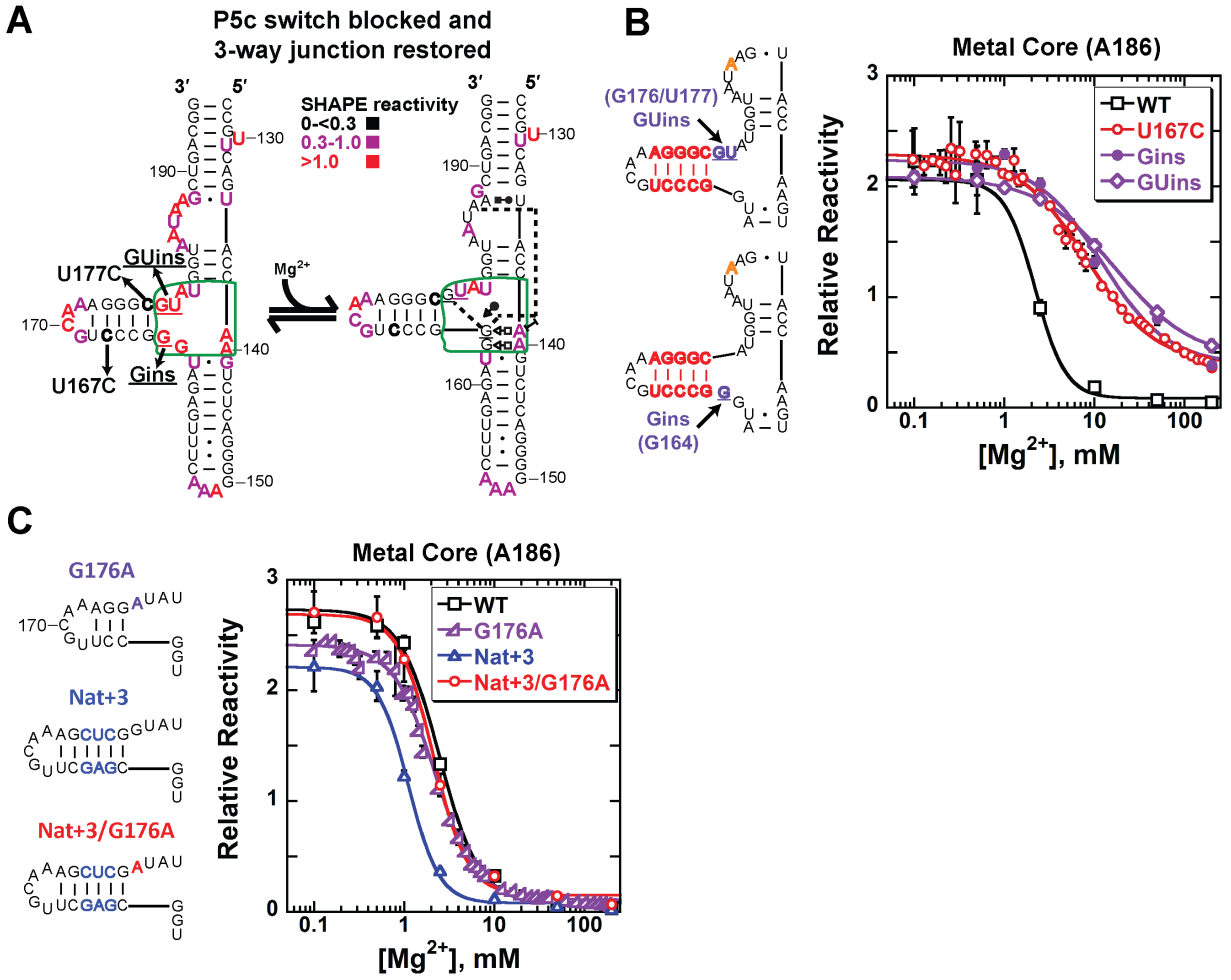

Figure S5. Module-level restoration of tertiary structure formation. Related to Figure 5

(A) Folding of the construct in which tertiary structure formation in the 3WJ and MC is restored by insertions of G164, G176, and U177 equivalents. The figure shows the SHAPE reactivity pattern in the absence of Mg^{2+} (left) and in the presence of saturating Mg^{2+} (right, 50–200 mM Mg^{2+}).

(B) Insertion of nucleotides on one strand or the other of the connection between P5c and the 3WJ (G164 or G176/U177 equivalents) is not sufficient to rescue MC formation, relative to the absence of the insertions in a construct that stabilizes the alternative secondary structure of P5c (U167C).

(C) The G176A substitution destabilizes tertiary structure, supporting involvement of G176 in tertiary structure formation with the 3WJ. The G176A substitution was shown previously to stabilize the native secondary structure (Gracia et al., 2016; Xue et al., 2016) (secondary structures at left). Surprisingly, we found that G176A does not stabilize formation of the MC, as indicated by protection of A186 (purple curve, at right), but instead gives an indistinguishable Mg^{2+} from that of the wild-type P5abc (black). This was surprising because the simplest model would have been that the stabilization of native secondary structure by G176A would have reduced the Mg^{2+} requirement for tertiary structure formation. To test for the possibility of a destabilizing effect of G176A on tertiary structure, we separated out effects on secondary structure by measuring the effect of G176A in the background of a second mutation that enforces the native secondary structure. In this background, the G176A substitution increases the Mg^{2+} requirement for MC formation (red vs blue), indicating that the G176A substitution destabilizes tertiary structure formation in the MC.

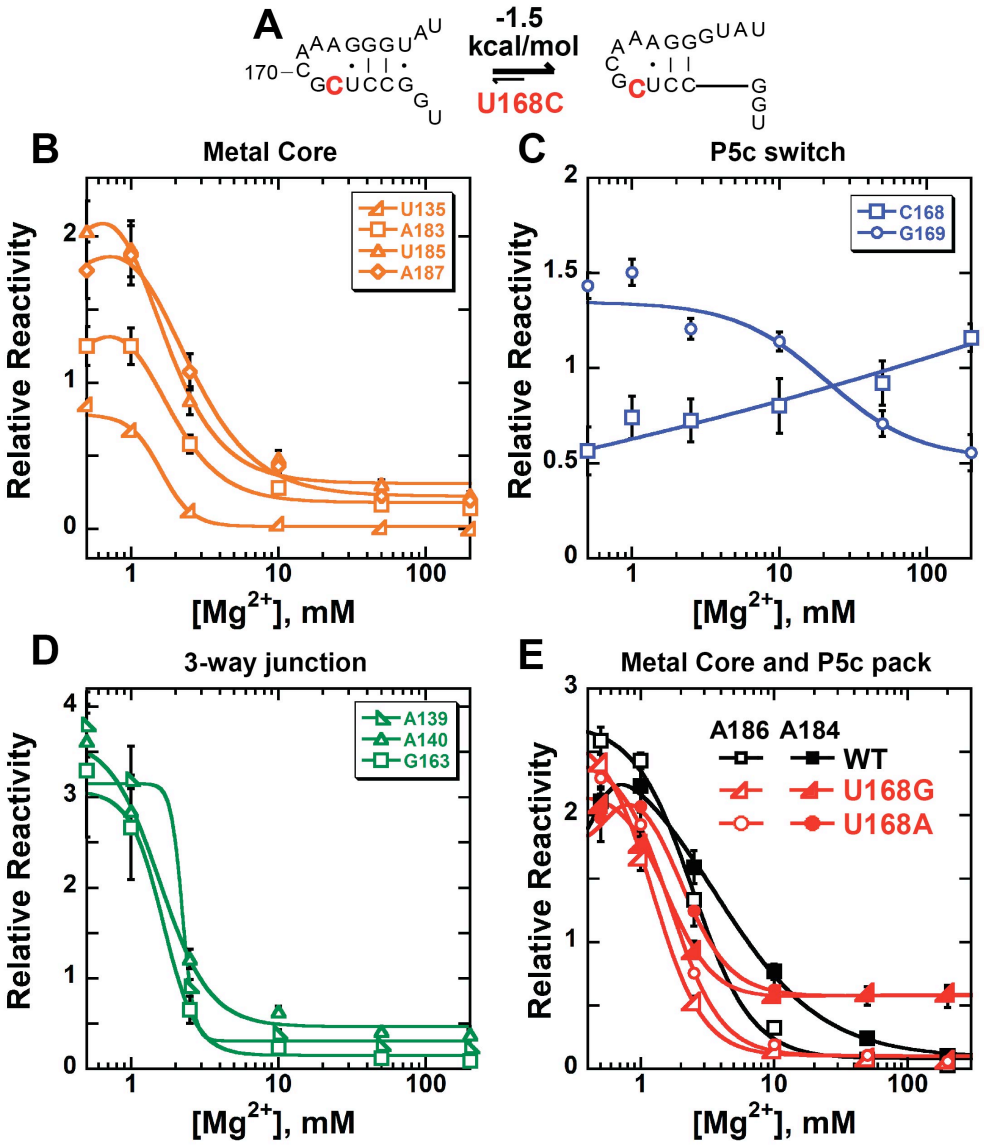

Figure S6. Mutation of U168 perturbs the P5c packing transition but does not affect MC formation. Related to Figure 6

(A) The mutation U168C is predicted to favor the native P5c secondary structure by 1.5 kcal/mol relative to the wild-type sequence of P5c.

(B–D) Folding of mutant U168C by SHAPE. Data in panel B show that the metal core forms at least as efficiently as in the wild-type P5abc. Data in panel C show the absence of protections at U168 and G169, relative to wild-type P5abc, suggesting that P5c does not pack efficiently with the MC. Data in panel D show that the 3WJ forms at least as efficiently as in the wild-type P5abc. Thus, the defective folding is specifically in the P5c packing step.

(E) Additional mutations of U168 (U168G and U168A) block the P5c packing transition (A184, closed symbols) but do not affect the lower Mg^{2+} transition (A186, open symbols). Note that A184 also undergoes a protection in the lower Mg^{2+} transition, and the defect in P5c packing is indicated by the lack of further protection in A184 at higher Mg^{2+} concentrations.

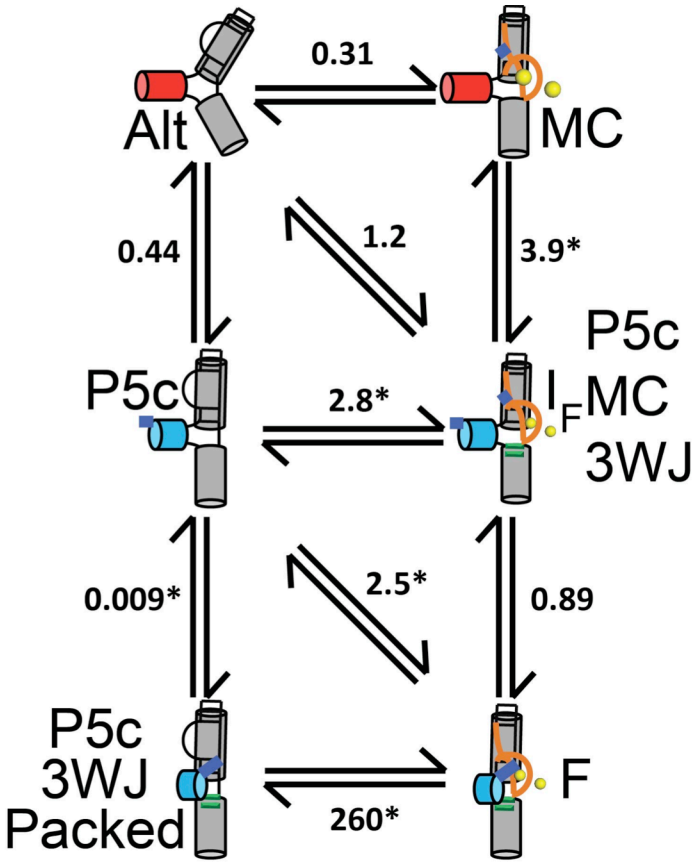

Figure S7. Quantitating the cooperativity between P5c packing and the MC. Related to Figure 7
Thermodynamic framework for MC folding, P5c secondary structure switching, and P5c packing. Values are measured at 3 mM Mg^{2+}. Calculated values are indicated with an asterisk (*). Note that the species that are populated for equilibrium folding of wild-type P5abc and depicted in Figure 7 are Alt (top left), I_F (middle right) and F (bottom left).

Table S1. Mg^{2+}-dependent folding parameters from SHAPE footprinting. Related to Figure 3 (The table is in a separate Excel file due to its large size)

Table S2. Mg^{2+}-dependent folding parameters from DMS footprinting. Related to Figure 3

Wild-type	**Region**	**Change**	**$[Mg^{2+}]_{1/2}$, mM**	**Hill, n**	**Amp, A**
A173	P5c	Enhancement	20 ± 10	0.92 ± 0.09	0.96 ± 0.16
A183	MC	Protection	15 ± 4	1.4 ± 0.4	1.1 ± 0.2
A184	MC	Protection	14 ± 5	1.8 ± 0.4	0.73 ± 0.07
A186	MC	Protection	5.9 ± 1.7	2.0 ± 0.1	1.1 ± 0.2
A187	MC	Protection	6.8 ± 1.7	1.6 ± 0.2	0.86 ± 0.06
WT, 5% DMSO	**Region**	**Change**	**$[Mg^{2+}]_{1/2}$, mM**	**Hill, n**	**Amp, A**
A173	P5c	Enhancement	15 ± 1	0.78 ± 0.10	1.4 ± 0.21
A183	MC	Protection	12 ± 5	0.96 ± 0.22	1.3 ± 0.3
A184	MC	Protection	9.6 ± 2.8	1.0 ± 0.2	0.80 ± 0.08
A186	MC	Protection	2.9 ± 0.3	1.6 ± 0.4	1.1 ± 0.2
A187	MC	Protection	3.9 ± 0.5	1.4 ± 0.1	0.78 ± 0.06
A:U	**Region**	**Change**	**$[Mg^{2+}]_{1/2}$, mM**	**Hill, n**	**Amp, A**
A173	P5c	Enhancement	3.4 ± 0.8	1.1 ± 0.1	1.0 ± 0.2
A183	MC	Protection	77 ± 3	2.1 ± 0.3	0.69 ± 0.01
A184	MC	Protection	23 ± 8	0.81 ± 0.23	0.59 ± 0.12
A186	MC	Protection	3.2 ± 0.4	0.88 ± 0.02	0.71 ± 0.03
A187	MC	Protection	7.3 ± 2.3	0.70 ± 0.05	0.78 ± 0.16
A:U/A186U	**Region**	**Change**	**$[Mg^{2+}]_{1/2}$, mM**	**Hill, n**	**Amp, A**
A173	P5c	Enhancement	455 ± 17	0.98 ± 0.03	0.95 ± 0.05
A183	MC	NC	NC	NC	NC
A184	MC	NC	NC	NC	NC
U186	MC	RTS	RTS	RTS	RTS
A187	MC	NC	NC	NC	NC

Nucleotides that do not change are labeled as NC. Positions that have reverse transcription stops are labeled as RTS.

Table S3. Parameters from global modeling. Related to Figure 3

Model	K_1	K_2	K_3	K_4	$\chi 2$
4 state, A-B coop	0.042	11	0.98	NA	30.1 ± 0.2
4 state, B-C coop	0.28	2.7	2.0	NA	63.7 ± 0.2
5 state, A-B coop	0.04	1.2	2.1	12	16.0 ± 0.1
5 state, B-C coop	0.5	2.4	1.9	9.1	14.7 ± 0.1
5 state, C-D coop	2.8	28	0.097	3.0	30.3 ± 0.2

See *Supplemental Experimental Procedures* for the initial constraints of each global fit. NA, not applicable for the model.

Supplemental Experimental Procedures

Global modeling of SHAPE and DMS footprinting data: We imported 29 sets of quantified SHAPE and DMS footprinting data from the wild-type P5abc into Kintek Kinetic Explorer and fit all of the data using one global model (Johnson et al., 2009). The global modeling was evaluated by minimizing the χ^2 value of the fit (defined as the sum of the residuals squared, assuming a constant sigma value for all data points). As described in Results, the simplest model that adequately described the data included four P5abc conformations, or states, with three Mg^{2+}-dependent transitions between them. From inspection of the data, it was clear that at least one of these transitions, centered at approximately 2 mM Mg^{2+}, gave steeper dependences than would be possible for binding of a single Mg^{2+} ion. To enable one of the transitions to be cooperative with respect to Mg^{2+} binding, which is not explicitly allowed in the Kinetic Explorer software, we incorporated an additional state into the model, making a total of five states (Scheme 1). The goal in including this 'extra' state was that it would not be populated significantly at any Mg^{2+} concentration but would allow a single transition to involve binding of two Mg^{2+} ions. Thus, for example state B could bind a Mg^{2+} ion to progress to state C, which would not be populated because state C would then bind an additional Mg^{2+} ion with higher affinity to progress to state D. Note that this transition likely involves the uptake of two site-bound Mg^{2+} ions that are associated with the folded MC (Das et al, 2005), but the dependence indicates only the net uptake of two Mg^{2+} ions, which could bind to specific sites or become part of the delocalized ion atmosphere.

$$A \leftrightarrow B \leftrightarrow C \leftrightarrow D \leftrightarrow E \qquad \text{(Scheme 1)}$$

$$\text{Reactivity} = sa1*A + sb1*B + sc1*C + sd1*D + se1*E \qquad \text{(Equation 1)}$$

As indicated in eq. 1, the observed reactivity for each nucleotide is defined as a linear combination of scaling factors associated with each state. In the global fitting, the scaling factors for each nucleotide were allowed to vary for each state except the non-populated state within the transition that is cooperative with Mg^{2+} binding. The scaling factors for the non-populated state were constrained to be equal to those of the state preceding it, and both of these scaling factors were locked to reasonable values prior to the fitting. In the model of Scheme 1, there are three possibilities for this folding step: the transition from A to C, from B to D, or C to E. We tested these possibilities individually by systematically requiring the scaling factors of each nucleotide to be the same for states A and B (sa1=sb1), for states B and C (sb1=sc1), or for states C and D (sc1=sd1). This constraint was applied to mimic the condition of a single transition by preventing the artificial intermediate state from having a unrealistically high scaling factor and consequently contributing to the overall signal in the transition region despite being at most sparsely populated. After global fitting under each constraint, the condition where state C is not significantly populated (five states, with the cooperative transition from state B to state D) produced a global fit that best described the data (Figure S1; Table S3).

We tested whether a simpler model could adequately describe the data by decreasing the number of states to four, one of which would again be a non-populated state included to allow one transition to be cooperative with Mg^{2+} concentration. We systematically constrained the scaling factors to allow each transition, in turn, to be the cooperative one, and we performed global fits to the data for the wild-type P5abc as above.

$$A \leftrightarrow B \leftrightarrow C \leftrightarrow D \qquad \text{(Scheme 2)}$$

$$\text{React} = sa1*A + sb1*B + sc1*C + sd1*D \qquad \text{(Equation 2)}$$

Global fitting under constraints to allow the first transition to be cooperative with Mg^{2+} concentration (*i.e.* sa1=sb1) converged on a model that fit poorly and in which the first two transitions were non-cooperative, as $K_1 < K_2$ (K_1 = 0.042 mM Mg^{2+}, K_2 = 11 mM Mg^{2+}; Table S3). When the second folding step was allowed to be cooperative with Mg^{2+} concentration, the resulting model did include this cooperativity, as indicated by a smaller value of K_3 than K_2 (K_2 = 2.7 mM Mg^{2+}, K_3 = 2.0 mM Mg^{2+}; Table S3), but this model was unable to accommodate the large changes in signal at Mg^{2+} concentrations in the range of 10 mM, resulting in a poor overall fit, as indicated by a high χ^2 value (Table S3). Thus, the best fit to the data included a total of four 'real' states, with an additional fifth state included in the model to allow for one of the transitions to be cooperative with Mg^{2+} concentration (Scheme 1).

Assignment of the transition that increases the DMS reactivity of A173: An interesting feature of the footprinting data was the enhanced DMS reactivity of A173, which suggests a tertiary-contact-induced transition from a Watson-Crick pair of U167-A173 to the non-canonical pair observed in the crystal structure. This DMS enhancement at A173 was suggested previously to monitor the secondary structure change of P5c (Silverman et al., 1999), but we conclude that it instead reflects P5c tertiary packing for two reasons. First, its Mg^{2+} dependence is the same as that for other nucleotides in the P5c packing transition (Figure 2F, A184 and G188) and different from those in the secondary structure change (Figure 2E, U168 and G169 enhancements at 1 mM). Second, the secondary structure change is not expected to enhance the DMS reactivity of A173. A173 remains paired, switching its partner from U168 to U167, and the ^{15}N chemical shift of U167 in the excited state suggests a Watson-Crick pair between U167 and A173 (Xue et al., 2016). DMS footprinting of the P4-P6 domain, the folded and assembled P5abc ribozyme core complex, and the full-length, folded ribozyme show that A173 is strongly reactive to DMS (Gracia et al., 2016; Murphy and Cech, 1993; Tijerina et al., 2007), suggesting that the fully folded and packed state we observe is the native conformation of P5abc present in the intact intron.